Production and diffusion of H_2O_2 during the interaction of a direct current pulsed atmospheric pressure plasma jet on a hydrogel

Manikandan Suresh, V. S. Santosh K. Kondeti and Peter J. Bruggeman

Department of Mechanical Engineering, University of Minnesota, Minneapolis, MN, 55455, USA

E-mail: pbruggem@umn.edu

23 January 2022

Abstract.

The interaction of cold atmospheric pressure plasma jets with hydrogels has been used as a model system to study the interaction of plasmas with tissues. In this study, we analyze the diffusion of reactive oxygen species (in particular H_2O_2) and quantify the amount of plasma-produced H_2O_2 species that penetrates into a gelatin hydrogel. We show that the diffusion constant of H_2O_2 in 10% gelatin hydrogel is similar to its diffusion constant in water and that the production of H_2O_2 in the hydrogel is significantly less than the production of H_2O_2 in distilled water for the same plasma operation conditions suggesting that the scavenging of OH radicals at the plasma-gel interface significantly reduces the H_2O_2 production.

1. Introduction

Low temperature plasmas (LTP) enable the production of chemically rich environments at ambient temperatures and pressures [1]. Hence, LTP containing air can deliver reactive oxygen and nitrogen species (RONS) in a non-destructive and beneficial way to heat sensitive substrates [2]. In the last decade, it was shown that the direct application of plasma to heat sensitive living tissues/surfaces and the associated RONS have the potential to cure a range of ailments such as wound healing, cancer treatment and dental hygiene [3]. Plasma-generated RONS play a key role in plasma medicine and are known to be responsible for regulating the key biological pathways which are known to cause the chemical and physical changes in organisms [4]. Experiments and research clearly indicate the impact of RONS in cell proliferation, migration and angiogenesis, pathogen inactivation in decontamination applications, apoptoses and necroses in plasma-enabled cancer treatment and determine the mechanisms involved in the plasma bio-interactions [2, 3, 5]. A detailed understanding of the production of these species and the control of their generation are just emerging and continue to be explored actively [6–8].

As plasma-medical applications often involve the direct interaction of plasma with biological cells, tissues and organisms, a strong coupling between the biological substrate and the plasma can exist that directly impacts the reactive species generation and species flux to the biological substrate [9]. A better understanding of this interaction and the associated species fluxes will enable the control of plasma-bio interactions and a safer and more effective implementation of plasmas for medical treatments. As many plasma-produced RONS are highly reactive, transport of these RONS in biological substrates lead to species gradients with penetration depths

depending on species lifetime. A detailed understanding of these underpinning transport phenomena and limitation becomes exceedingly important in the context of plasma medicine [10].

Detailed studies of the physical interaction of plasma with living tissue is challenging due to the intrinsic sample-to-sample variability and the high cost of lab grown tissues. Hence, in the last decade a growing effort on artificial tissue models have been explored [11]. Gelatin and agarose gels are often considered as models for artificial tissue [11–13]. An additional advantage is that these gels are optically transparent enabling loading of chemical indicators [11,14–16]. For example, Szili *et al* and Kawasaki et al reported the transport of plasma-generated reactive oxygen (ROS) species through gelatin and agarose gels with a thickness of 1 mm showing the ability of ROS to penetrate on these length scales through gel [11,12]. Furthermore, a spatial temporal measurement of the impact of ozone on gels was performed by Liu *et al* for He + 0.5% O_2 plasma [15]. Interestingly, a linearly decreasing trend of penetration depths with increasing mass fractions of gelatin was found clearly indicating the reactions of plasma produced RONS with the gel matrix or impaired diffusion caused by the increasingly denser matrix. Using similar techniques as Liu et al, Kawasaki et al showed typically ROS transport time scales in the gel of 0.14-0.2 mm/min [16].

While a few dozens of papers on plasma-gel interaction with chemical indicators have been reported with a strong focus on RONS, quantitative analysis of these results to enable the determination of the amount of RONS supplied to the gel or the determination of diffusion constants remains highly limited. To our knowledge, the only quantitative analysis of plasma-induced changes in the hydrogel is the measurement of pH profiles by Busco *et al* [18] with a pH indicator added to the hydrogel. A recent review addresses remaining challenges for plasma-hydrogel

interactions, cited diffusion effects and a direct correlation between ROS and chemical indicators as unexplored aspects in the reviewed literature [13]

The objective of this study is to analyze the diffusion of ROS (in particular H_2O_2) and quantify the amount of plasma produced H_2O_2 species that penetrates into a gelatin hydrogel, as a model for the tissue. Furthermore, the flux of plasma generated H_2O_2 species both in liquid medium (distilled water) and gelatin hydrogel are determined. The latter is particularly important as the measurement of H_2O_2 fluxes at the plasma-gel interface is complex. Diagnostics such as molecular beam mass spectroscopy do not allow measuring *in situ* species fluxes without impacting the properties of the gel substrate and ultimately the plasma properties and the flux of H_2O_2 [19]. In addition, H_2O_2 has a very small absorption cross section and requires multi-pass absorption or cavity ring down spectroscopy (CRDS) [20,31] methods with limited spatial resolution that are particularly challenging for small plasmas.

2. Methods

2.1. Plasma setup

Figure 1 shows the plasma jet used for studying plasma-gel interactions. The plasma jet consists of a high voltage tungsten needle electrode with a diameter of 1 mm surrounded by a quartz tube with an inner diameter of 2 mm and an outer diameter of 3 mm. A copper ring ground electrode with a height of 5.25 mm was placed around the quartz tube at a distance of 5 mm from the tip of the nozzle such that the tip of the needle is in the middle of the ring electrode. He, He + 0.81% H_2O and He + 0.8% O_2 at a flow rate of 1 standard litres per minute (slm) controlled by a mass flow controller (MKS GE50A) were used as the feed gas. A 4 kV DC voltage was generated

by a positive polarity DC power supply (Spellman SL300). A pulse generator (DEI PVX-4110) gated by a function generator (Tektronix AFG 2021) was used to generate the 4 kV, 200 ns, 5 kHz voltage pulses. A 1 kΩ resistor was incorporated in the circuit in order to limit the current and keep the gas temperature close to room temperature. The output of a Rogowski coil (Pearson 2877) and a voltage probe (Tektronix P6015A) were recorded with an oscilloscope (RIGOL 1204B) A schematic of the electrical circuit is shown in Figure 1. The plasma jet was operated in ambient air. The temperature of the lab was 21° - 22° C and the relative humidity of the ambient air in the lab was 30%. Figure 1 also shows how the jet was impinging on the gel sample. The gel substrate was floating in the treatments.

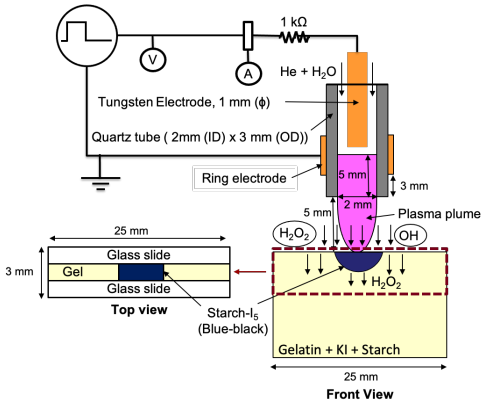

Figure 1. Schematic of the plasma jet used in this study while interacting with a gelatin hydrogel sample. The diffusion of H_2O_2 into the gel is schematically depicted by the blue color, representing the change of color of the chemical indicator, in front and top views. The voltage and current probe are indicated by V and A, respectively.

2.2. Hydrogel preparation

A gelatin hydrogel sample (10% weight/volume) was used in this work motivated by several studies reporting plasma-hydrogel interactions for these conditions as reviewed in [13]. One gram gelatin was mixed with 4 mL distilled water and incubated at room temperature for 15 minutes. Simultaneously, 6 mL of distilled water containing a given concentration of chemical indicator (see further) was warmed at 60° on the heater for 15 minutes. The heated solution was added to the gelatin/water mixture. The resulting 10% gelatin/water mixture was stirred at 1000 rpm for 10 minutes using a magnetic stirrer. The solution was stirred for another 10 minutes at 250 RPM. Stirring the solution prevents coagulation of the gelling material and acts as a prerequisite to form a consistent homogeneous hydrogel. The prepared hydrogel mixture was injected with the help of a pipette (Eppendorf research plus: 100 - 1000 μL) in between two parallel microscopic glass slides (thermo scientific GOLD SEAL: 25×75 mm, 1 mm thick) separated by a thickness of 1 mm using a third microscopic glass slide placed in between them. The thickness of the resulting 1 mm solution layer was small to ensure the gelling material remained between the glass plates due to its own viscosity. The samples were cooled at room temperature and subsequently refrigerated for 1 day before being used in the experiments.

2.3. Chemical indicators

Inspired by the work of Kawasaki *et al* [16], potassium iodide (KI)-starch was added to the hydrogel as chemical indicator in this work. KI-starch is a commonly used indicator for H_2O_2 detection [21]. The reaction is however a multi-step process and

non-selective. First iodide is oxidized and converted to iodine as follows [21]:

$$H^+ + I^- + H_2O_2 \longleftrightarrow HIO + H_2O \tag{1}$$

$$I^- + HIO + H^+ \longleftrightarrow I_2 + 2H_2O \tag{2}$$

The iodine molecule (I_2) further reacts with iodide (I^-) to form the triiodide molecule (I_3^-). Finally, the triiodide reacts with starch to form a starch-pentaiodide complex causing the observed blue-black color [21].

$$I_2 + I^- \longleftrightarrow I_3^- \tag{3}$$

$$2I_3^- + \text{starch} \longrightarrow \text{starch-}I_5 + I^- \tag{4}$$

Reaction 1 has a much smaller reaction rate coefficient than the subsequent reactions and is typically the rate limiting step for the formation of the blue-black colored complex [21], at least in cases where there are no side reactions. Plasmas produce several other oxidizing species including ozone, O and OH that are more potent oxidizers than hydrogen peroxide. We checked the role of OH in the starch-I_5 complex formation in water by comparing a solution with H_2O_2 only and the same solution with added Fe_2^+ to enable the formation of OH radicals through Fenton's reaction [22]. The faster formation of the starch-I_5 complex was observed in this case, illustrating that radical reactions can contribute to the starch-I_5 complex formation.

In order to prepare 10 mL of 0.3% KI-starch indicator solution 30 mg of KI was mixed with 5 mL of 1% starch solution and 5 mL of distilled water. The color change observed during the plasma treatment and H_2O_2 droplet experiments were recorded using a CCD camera (Nikon D3100). The camera was fixed on a mount and focused manually on to the region of interest using an objective lens. The distance between the camera and the sample was made reproducible using a fixed mount for the samples.

The images were recorded with a white paper background at standard laboratory lighting conditions with a fixed exposure of 1/60 s and an aperture of f/8.

We measured H_2O_2 in water with a colorimetric approach using $TiOSO_4$ reagent [21]. As the plasma also produces HNO_2, which can react with H_2O_2, and reduce the H_2O_2 concentration post-treatment [23], a 133 µL solution of 60 mM NaN_3 was added to 1 mL of the liquid sample to quench the reactive nitrogen species that could interfere with the H_2O_2 concentration measurement. The H_2O_2 measurement was performed as in Ref. [24].

3. Results

Figure 2 shows the voltage and current of He + 0.8% H_2O plasma jet operated in open atmosphere. The profile of the voltage and current waveforms of the He and He+ 0.8% O_2 plasmas were similar to the He + 0.8% H_2O plasma shown in figure 2. The energy obtained by integrating the product of current and voltage is also

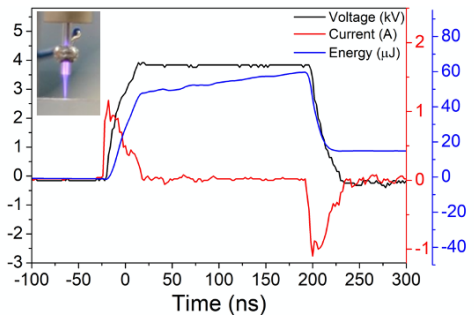

Figure 2. The measured current and voltage for He + 0.81% H_2O plasma jet. The energy is obtained by integrating the product of the current and the voltage with upper boundary the respective time on the horizontal axis. The inset shows the image of the plasma interacting with the gel sample. The nozzle to substrate distance is 5 mm.

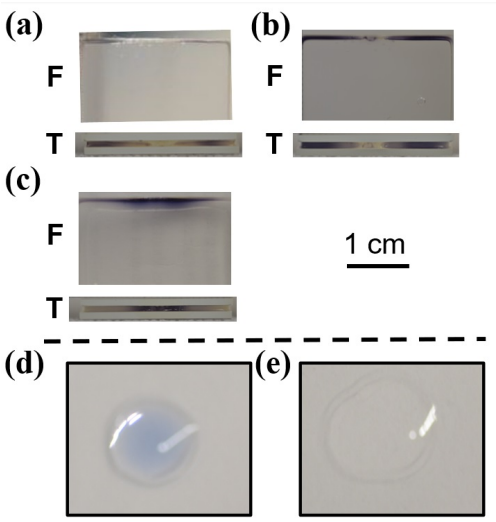

Figure 3. (a-c) Front view (F) and top view (T) of the plasma treated hydrogel sample. (a) Dry He, (b) He + 0.8% O_2 and (c) He + 0.81% H_2O. (d-e) Images of 20 µL solution of 0.03% KI + 0.05% starch + 1 mM H_2O_2. (d) Untreated droplet and (e) droplet after 30 s treatment by He plasma.

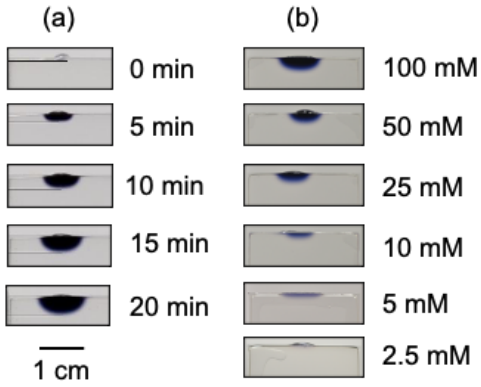

Figure 4. Images depicting the penetration of H_2O_2 into hydrogel containing 180 mM KI-starch. A droplet of 8 µL H_2O_2 was placed on top of the gel. (a) Penetration as a function of time for 1 M H_2O_2 droplet and (b) Penetration after 20 min as a function of the H_2O_2 concentration in the droplet.

shown. As the total current is used to calculate the power and energy, the energy needed to charge and discharge the capacitance of the plasma jet is subtracted from the total energy to obtain the plasma dissipated energy. While the energy to charge the capacitance is 40 μJ,the plasma dissipated energy per pulse is only 15 μJ. The jet operating in He and He + 0.8% O_2 have a larger plasma dissipated energy of 50 μJ and 20 μJ respectively. The gas temperature increase in the same jet operating at 50 μJ was reported to be 15 K although for the jet impinging on a glass substrate [25]. While plasma-induced gel deformations upon plasma treatment have been reported [11], this was not observed for the conditions reported in this work. The stability of the gel might have been enhanced by the glass slides.

Plasma produces several other oxidizing species including ozone, O and OH that are more potent oxidizers than hydrogen peroxide. While the blue-black complex can be formed by the reaction of KI starch with OH and H_2O_2 (see section 2.3), the moderate oxidation potential of H_2O_2 suggest that several other plasma-produced oxidizing species can cause the oxidation of I^-. Hence, we compared the effect of the plasma jets operating in 3 different gas environments on a KI starch loaded hydrogel to qualitatively assess the role of different oxidizing species (O, O_3, OH and H_2O_2) that might enable the oxidation of I^- to I_2. No change in the color of the hydrogel was observed when the plasma was not visibly in contact with the hydrogel (not shown). Figure 3 (a), (b) and (c) show the front and top views of the gel treated by dry He, He + 0.8% O_2 and He + 0.8% H_2O plasmas respectively when the plasma was in contact with the hydrogel. A blue-black color was clearly visible after all the three different feed gas plasma treatments and confirms the formation of the starch-I_5 complex. In the case of He + 0.8% H_2O, the blue-black complex was formed both directly below the core feed gas flow and in the region surrounding the core feed gas flow. However,

the treatment by He or He + 0.8% O_2 plasma shows that the region surrounding the core feed gas has more net starch-I_5 complex formation compared to the central region directly below the plasma jet effluent (Figure 3 (a), (b)). This suggests that the species produced by the diffusion of ambient air from the surroundings into the plasma plume results in the production of reactive species responsible for the formation of the starch-I_5 complex. The diffusion of O_2 or water vapor from the ambient atmosphere can result in the production of reactive oxygen species such as O, O_3, OH and H_2O_2. He + 0.8% O_2 plasma generates copious amounts of O and O_3 in the core region of the feed gas flow [19]. The lack of formation of starch-I_5 complex at the interface between the plasma and the gel suggests that short-lived species such as O atoms do not result in the formation of a significant amount of the blue-black complex or the radical species flux is large enough to cause decomposition of the starch-I_5 complex. In addition, the starch-I_5 complex formation seems to be limited to the plasma-gel interface. The fact that the blue-black complex was formed directly below the core feed gas flow in the case of H_2+0.8% H_2O does not mean that no destruction reactions of the blue-black complex are occurring, it only allows to conclude that the production reaction is significantly faster than the destruction reaction and/or the species responsible for the destruction reaction do not significantly penetrate into the gel while the species responsible for the production of the blue-black complex have this ability.

To assess the possibility of starch-I_5 complex destruction by the plasma action, a solution of 0.03% KI + 0.03% starch + 1 mM H_2O_2 was prepared. The reaction of starch-I_5 complex with iodide was allowed to proceed for an hour to ensure that all the H_2O_2 was consumed to form the blue-black complex. This concentration combination of KI, starch and H_2O_2 was chosen as a condition where the least, but still visible blue-black color is formed. Figure 3 (d) shows a 20 μL droplet of this solution. When

this droplet was treated by a He plasma, the blue-black color disappeared (3 (e)). This result confirms that the reactive species from the plasma can destroy the formed blue-black complex, in addition to forming the blue-black complex. Hence, the lack of the starch-I_5 complex formation below the core gas flow for He and He + 0.8% O_2 plasmas is likely due to the destruction of the formed blue-black complex.

Another key distinctive feature different between He + 0.8% H_2O plasma and He and He + 0.8 % O_2 plasma gel interaction, is that the penetration depth of the blue-black color into the gel is larger for He + 0.81% H_2O (Figure 3 (a), (b) and (c)). Water containing plasmas are a major source of H and OH radicals [26]. In addition, the He + 0.8% H_2O plasma will be a more abundant source of H_2O_2 [27]. O radicals have been reported to show a similar reactivity as OH radicals in solution [28]. The high reactivity of OH, charged species, excimer radiation and O radicals is expected to lead to a limited penetration of a few micrometers into the hydrogel due to the large concentrations of organic molecules (gelatin and starch). Reactions induced by ozone in gels for a large range of conditions do not penetrate more than 500 μm [15]. However, H_2O_2 is a long-lived species and its lower reactivity with organic molecules is expected to allow for a deeper penetration into the hydrogel. Figure 4 shows the formation of the starch-I_5 complex as a function of time after placing an 8 μL droplet containing 1 mM H_2O_2 on top of the hydrogel. The blue-black color penetrates deeper into the hydrogel with the passage of time. Hence the enhanced production of H_2O_2 by the He + 0.8% H_2O plasma is consistent with the larger observed penetration of the blue-black color compared to He and He + 0.8% O_2 plasmas.

Figure 4 (b) shows the penetration of the blue-black color 20 minutes after placing an 8 μL droplet with different concentrations of H_2O_2 placed on top of the hydrogel. The H_2O_2 from the droplet penetrates into the hydrogel and these results can serve

as a calibration for the plasma-produced H_2O_2 in the hydrogel as shown in Figure 3 (c). A direct comparison between the H_2O_2 droplet and the plasma jet treatment with He+0.8% H_2O is only possible if H_2O_2 is also dominantly responsible for the plasma-induced blue-black complex formation. While the near interfacial layer can be impacted by other species such as O_3, H, O and OH, the ROS penetration occurring for distances more than 500 μm is due to H_2O_2. The direct comparison of the penetration depth suggests that the plasma generates as a droplet containing between 0.04-0.08 μmoles of H_2O_2 (i. e. 5 and 10 mM case). The amount of H_2O_2 produced for the same plasma upon treatment of 1.5 mL distilled water was 0.8 μmoles H_2O_2. This 10 to 20 times larger H_2O_2 production is very similar to the ratio of H_2O_2 fluence through a liquid layer as obtained by modeling for a touching and non-touching plasma jet [29]. This difference in the model is ascribed to photolysis and charge-exchange reactions leading to OH radical formation, a precursor for the formation of H_2O_2. Similar reactions will lead to OH formation in the hydrated gel but the formed OH radicals will readily react with gelatin (and starch) that is present at large concentrations. While the interaction of plasma with water and hydrogel is expected to be similar, the differences cannot be fully excluded which prevent a more detailed quantitative comparison of the H_2O_2 production.

Figure 4 (a) allows us to analyse the transport of H_2O_2 into the hydrogel. We established that the starch-I_5 complex does not diffuse significantly in the hydrogel on the timescale of our study. Hence, we can estimate the effective diffusion constant (D) of H_2O_2 through the relation for linear diffusion in 1 dimension:

$$\tau_{\mathrm{D}} = \frac{\Lambda^2}{D} = \frac{l^2}{\pi^2 D} \tag{5}$$

with τ_{D} the diffusion time, Λ the diffusion length and l the length of color formation.

We checked that the diffusion is not sensitive to the hydrogen peroxide concentration in the droplet and found that the diffusion coefficient is equal to $1.2 \pm 0.3 \times 10^{-9}$ $m^2 s^{-1}$. Within the experimental accuracy, this value is equal to the diffusion coefficient in water of H_2O_2 (1.4×10^{-9} $m^2 s^{-1}$ [30]). This suggests that the diffusion of H_2O_2 is not significantly impacted by the reaction of H_2O_2 with I^- or the gelatin in the hydrogel. The timescale for diffusion across a distance of 1 mm is equal to 84 ± 23 s. The reaction rate at neutral conditions for H_2O_2 with I^- is 0.0115 Ms^{-1} [21]. Hence, for 180 mM KI, it yields a reaction timescale of 320 s which is 4 times slower than the diffusive transport.

The effective diffusion time constant determined from the experiment is actually an effective time constant as it includes the effect of reaction losses. When including the reaction loss in the diffusion equation the effective time constant can be related to the diffusion and reaction time constant τ_r as follows:

$$\frac{1}{\tau_{eff}} = \frac{1}{\tau_D} - \frac{1}{\tau_r} = \frac{1}{\tau_D} - k n_{I^-}. \tag{6}$$

where k is the effective reaction rate coefficient of all reaction losses and n_{I^-} is the density of I^-. If we assume that the diffusion time constant in the gel is equal to that of water, we obtain an effective diffusion time constant of 93 s which corresponds to the experimentally determined effective diffusion time constant within the experimental accuracy. Hence, the diffusion of H_2O_2 at a rate close to the rate found in water explains the color formation and transport in the gel as observed in this experiment. The color formation cannot be due to the reactive species that readily react with the hydrogel or those that react much more rapidly with I^- than H_2O_2.

4. Conclusion

In this work, we analyzed the plasma produced H_2O_2 flux to a hydrogel, a model for tissues, and its diffusion through the hydrogel using KI starch as an ROS indicator. It was shown that reactive species from the plasma can both destroy generate the blue-black complex. This led to a distinctive lack of blue-black complex in the gel directly below the core feed gas flow for He and He + 0.8% O_2 plasmas but not for He + 0.8% H_2O plasmas. While KI starch is an non-specific ROS indicator, the results suggest that short-lived oxidizing species have limited penetration depth and that H_2O_2 is dominantly responsible for the bulk production of the starch-I_5 complex. We also showed that a comparison with the positive control measurements enabled us to determine the amount of plasma-produced H_2O_2 that is responsible for the starch-I_5 complex. The obtained diffusion constant of H_2O_2 in the hydrogel is $1.2 \pm 0.3 \times 10^{-9}$ m^2s^{-1}, equal to its diffusion constant in water within the experimental accuracy. The results reported in this work suggest that high resolution spatially resolved absorption measurements of the blue-black complex would allow to quantify the penetration of H_2O_2 in the gel. Nonetheless both transport of H_2O_2 and its reaction time scales with KI-starch occur on a timescale of minutes, similar to typical plasma treatment times and hence such measurements do not easily provide information of changes in plasma properties during the treatment.

5. Acknowledgements

This material is based upon work supported by the United States Department of Energy, Office of Fusion Energy Sciences, General Plasma Science Program under award number DE-SC0016053.

References

[1] P J Bruggeman, F Iza and R Brandenburg 2017 Foundations of atmospheric pressure non-equilibrium plasmas, *Plasma Sources Sci. Technol.* **26** 123002.

[2] T von Woedtke, S Emmert, H-R Metelmann, S Rupf, and K-D Weltmann 2020 Perspectives on cold atmospheric plasma (CAP) applications in medicine *Phys. Plasmas* **27** 070601

[3] G Y Park, S J Park, M Y Choi, I G Koo, J H Byun, J W Hong, J Y Sim, G J Collins, J K Lee 2012 Atmospheric-pressure plasma sources for biomedical applications, *Plasma Sources Sci. Technol.* **21** (4) 43001.

[4] I Adamovich, S Baalrud, A Bogaerts, P J Bruggeman, M Cappelli et al 2017 The 2017 Plasma Roadmap: Low temperature plasma science and technology, *J. Phys. D. Appl. Phys.* **50** (32) 323001.

[5] D Dobrynin, G Fridman, G Friedman, and A Fridman 2009 Physical and biological mechanisms of direct plasma interaction with living tissue *New J. Phys.* **11** (11) 115020.

[6] J Jiang and P Bruggeman 2021 Tuning plasma parameters to control reactive species fluxes to substrates in the context of plasma catalysis *J. Phys. D: Appl. Phys.* **54** (21) 214005.

[7] T Ito, G Uchida, A Nakajima, K Takenaka and Y Setsuhara 2017 Control of reactive oxygen and nitrogen species production in liquid by nonthermal plasma jet with controlled surrounding gas *Jpn. J. Appl. Phys.* **56** 01AC06

[8] X Lu, G V Naidis, M Laroussi, S Reuter, D B Graves, K Ostrikov 2016 Reactive species in non-equilibrium atmospheric-pressure plasmas: Generation, transport, and biological effects *Phys. Reports* **630** 1-84

[9] T Darny, J-M Pouvesle, V Puech, C Douat, S Dozias and E Robert 2017 Analysis of conductive target influence in plasma jet experiments through helium metastable and electric field measurements, *Plasma Sources Sci. Technol.* **26** 45008

[10] X Lu, M Keidar, M Laroussi, E Choi, E J Szili, K Ostrikov 2019 Transcutaneous plasma stress: From soft-matter models to living tissues, *Materials Science & Engineering: R* **138** 36-59

[11] E J Szili, J W Bradly and R D Short 2014 A 'tissue model' to study the plasma delivery of reactive oxygen species, *J. Phys. D: Appl. Phys.* **47** 152002.

[12] T Kawasaki, G Kuroeda, R Sei, M Yamaguchi, R Yoshinaga, R Yamashita, H Tasaki, K Koga, and M Shiratani 2017 Transportation of reactive oxygen species in a tissue phantom after

plasma irradiation *Jpn. J. Appl. Phys.* **57** 01AG01

[13] M Thulliez, O Bastin, A Nonclercq, A Delchambre and F Reniers 2021 Gel models to assess distribution and diffusion of reactive species from cold atmospheric plasma: an overview for plasma medicine applications, *J. Phys. D: Appl. Phys.* **54** 463001.

[14] J-S Oh, E J Szili, N Gaur, S-H Hong, H Furuta, H Kurita, A Mizuno, A Hatta and R D Short 2016 How to assess the plasma delivery of RONS into tissue fluid and tissue, *J. Phys. D: Appl. Phys.* **49** 304005.

[15] D Liu, T He, Z Liu, S Wang, Z Liu, M Rong, M G Kong 2018 Spatial-temporal distributions of ROS in model tissues treated by a He+O_2 plasma jet, *Plasma Process Polym.* **215** e1800057.

[16] T Kawasaki, A Sato, S Kusumegi, A Kudo, T Sakanoshita, T Tsurumaru, G Uchida, K Koga and M Shiratani 2016 Two-dimensional concentration distribution of reactive oxygen species transported through a tissue phantom by atmospheric-pressure plasma-jet irradiation, *Appl. Phys. Express* **9** 076202.

[17] E J Szili, J-S Oh, S-H Hong, A Hatta, and R D Short 2015 Probing the transport of plasma-generated RONS in an agarose target as surrogate for real tissue: dependency on time, distance and material composition *J. Phys. D. Appl. Phys.* **48** (20) 202001.

[18] G Busco, A V Omran, L Ridou, J-M Pouvesle, E Robert and C Grillon 2019 Cold atmospheric plasma-induced acidification of tissue surface: visualization and quantification using agarose gel models, *J. Phys. D: Appl. Phys.* **52** (24) 24LT01.

[19] D Ellerweg, J Benedikt, A von Keudell, N Knake, and V Schulz-von der Gathen 2010 Characterization of the effluent of a He/O_2 microscale atmospheric pressure plasma jet by quantitative molecular beam mass spectrometry, *New J. Phys.* **12** (1) 13021.

[20] M Gianella, S Reuter, S A Press, A Schmidt-Bleker, J H van Helden, and G A D Ritchie 2018 HO_2 reaction kinetics in an atmospheric pressure plasma jet determined by cavity ring-down spectroscopy, *Plasma Sources Sci. Technol.* **27** (9) 95013.

[21] M C Milenković and D R Stanisavljev 2011 The kinetics of iodide oxidation by hydrogen peroxide in acid solution, *Russ. J. Phys. Chem. A* **85** (13) 2279–2282.

[22] V Kavitha and K Palanivelu 2004 The role of ferrous ion in Fenton and photo-Fenton processes for the degradation of phenol *Chemosphere* **55** (9) 1235-1243.

[23] P Lukes, E Dolezalova, I Sisrova, and M Clupek 2014 Aqueous-phase chemistry and bactericidal effects from an air discharge plasma in contact with water: evidence for the formation of

peroxynitrite through a pseudo-second-order post-discharge reaction of H_2O_2 and HNO_2 *Plasma Sources Sci. Technol.* **23** (1) 15019.

[24] V S S K Kondeti, C Phan, K Wende, H Jablonowski, U Gangal, J Granick, R C Hunter and P J Bruggeman 2018 Long-lived and short-lived reactive species produced by a cold atmospheric pressure plasma jet for the inactivation of Pseudomonas aeruginosa and Staphylococcus aureus, *Free Radic. Biol. Med.* **124** 275–287.

[25] E R W Van Doremaele, V S S K Kondeti, P J Bruggeman 2018 Effect of plasma on gas flow and air concentration in the effluent of a pulsed cold atmospheric pressure helium plasma jet, *Plasma Sources Sci. Technol.* **27** (9) 095006

[26] Y Yue, J Jiang, V S S K Kondeti and P Bruggeman (2021) Spatially and temporally resolved H and OH densities in a nanosecond pulsed plasma jet: An analysis of the radical generation, transport, recombination and memory effects, *J. Phys. D: Appl. Phys.* **54** 115202.

[27] C Vasko, D X Liu, E van Veldhuizen, F Iza and P Bruggeman 2014 Hydrogen peroxide production in an atmospheric pressure RF glow discharge: comparison of models and experiments, *Plasma Chem. Plasma Proc.* **34** 1081-1099.

[28] M M Hefny, C Pattyn, P Lukes and J Benedikt 2016 Atmospheric plasma generates oxygen atoms as oxidizing species in aqueous solutions, *J. Phys. D: Appl. Phys.* **49** 404002.

[29] S A Norberg, W Tian, E Johnsen and M J Kushner 2014 Atmospheric pressure plasma jets interacting with liquid covered tissue: touching and not-touching the liquid, *J. Phys. D: Appl. Phys.* **47** 475203.

[30] S A M van Stroe-Biezen, F M Everaerts, L J J Janssen, and R A Tacken 1993 Diffusion coefficients of oxygen, hydrogen peroxide and glucose in a hydrogel, *Anal. Chim. Acta* **273** (1–2) 553–560.

[31] M Djehiche, N L Le Tan, C D Jain, G Dayma, P Dagaut, C Chauveau, L Pillier and A. Tomas 2014 Quantitative measurements of HO_2 and other products of n-butane oxidation (H_2O_2, H_2O, CH_2O, and C_2H_4) at elevated temperatures by direct coupling of a jet-stirred reactor with sampling nozzle and cavity ring-down spectroscopy (cw-CRDS), *J. Am. Chem. Soc.* **136** 16689–16694.